Full Paper

Journal of the Brazilian Chemical Society

https://dx.doi.org/10.21577/0103-5053.20260081

J. Braz. Chem. Soc. **2026**, *37-Spe2*, e-20260081, 1-10

Synergistic Inhibition of Urease by Novel Chromene-Dihidropirimidinone Hybrids: A Combined Synthetic, Biological, and Molecular Dynamics Study

Samuel Jose Santos, [a] ***Luciana P. S. Viana,*** [b] ***Yasmin S. Coelho,*** [b] ***Nathalia M. L. Freire,*** [c] ***Thiago M. de Aquino,*** [c] ***Ângelo de Fátima*** [*,b,d] ***and Dennis Russowsky*** [*,a]

[a]*Laboratório de Sínteses Orgânicas, Instituto de Química, Universidade Federal do Rio Grande do Sul, 91501-970 Porto Alegre-RS, Brazil*

[b]*Grupo de Estudos em Química Orgânica Biológica, Departamento de Química, Instituto de Ciências Exatas, Universidade Federal de Minas Gerais, Pampulha, 31270-901 Belo Horizonte-MG, Brazil*

[c]*Grupo de Pesquisa em Estratégias Terapêuticas, Instituto de Química e Biotecnologia, Universidade Federal de Alagoas, Cidade Universitária, 57075-000 Maceió-AL, Brazil*

[d]*Department of Organic Chemistry, Faculty of Science, Atatürk University, 25240, Erzurum, Türkiye*

This study describes the design, synthesis, and biological evaluation of novel eight chromene-dihydropyrimidinone (Chro-DHPM) hybrids as urease inhibitors. The synthetic approach involved the covalent linkage of chromene and DHPM pharmacophores through a non-enolizable 1,2,3-triazole linker, efficiently constructed via the copper-catalyzed azide-alkyne cycloaddition (CuAAC) protocol. Evaluation of antiureolytic activity against urease from *Canavalia ensiformis* type III revealed that hybrids **4b** and **4h** were the most potent inhibitors, exhibiting 42.1 and 51.5% inhibition at 100 μM, respectively. These results were compared to thiourea (TIO), used as a positive control, which showed 63.5% inhibition under the same conditions. Furthermore, the hybrids demonstrated significantly enhanced activity compared to their individual precursors, chromene **1a** and Biginelli adducts **3b** and **3d**, thereby highlighting a synergistic effect from molecular hybridization. Molecular dynamics simulations of the most active hybrid, **4h**, elucidated a dual binding mechanism wherein the compound stabilizes within the urease active site through coordination of the tetrahydropyrimidine carbonyl oxygen to the binuclear nickel center, combined with steric occlusion of the catalytic entrance by the tetrahydro-4*H*-chromene moiety. Overall, this work demonstrates that molecular hybridization of chromene and DHPM scaffolds represents a promising strategy for developing novel antiureolytic agents.

Keywords: chromenes, dihydropyrimidinones, hybrid compounds, urease inhibitors, triazole linker

Introduction

The synthesis of hybrid compounds has emerged as a robust and versatile strategy in medicinal chemistry, enabling the development of novel pharmacological entities for the treatment of a wide range of human diseases, particularly cancer.[1-4] This approach moves beyond the traditional "one disease-one target-one drug" paradigm, shifting from single-target to multi-target drug design substantially expanded the scope of modern drug discovery, allowing for the development of ligands capable of simultaneously interacting with multiple biological targets, taking into account multifactorial disease etiologies frequently require more sophisticated and integrative therapeutic solutions.[5]

By covalently linking two distinct pharmacophores within a single molecular framework, hybridization strategies can give rise to new biological properties and finely modulated pharmacological activities, improving both therapeutic efficacy and safety.[6] In contrast to combination therapy or fixed-dose formulations, hybrid molecules often exhibit optimized pharmacokinetic profiles and a reduced risk of drug-drug interactions,

*e-mail: dennis@iq.ufrgs.br; adefatima.geqob@gmail.com
Editor handled this article: Giovanni Wilson Amarante (Executive)
This publication is part of the special issue "Organic Synthesis - BMOS"

as the pharmacological effects are delivered by a single chemical entity.[7]

Several literature reviews[8-10] were addressed to explore this strategy, discovering significant number of new hybrid compounds biologically active against different diseases, noteworthy the cancer. Our research has focused on the design and synthesis molecular scaffolds based on dihydropyrimidinones (DMPM) conjugate to different privileged pharmacophores addressed to fight against cancer.[11-16] More recently, chromene-dihydropyrimidinone (Chro-DHPM) hybrids were successfully investigated as a biofilm inhibitor,[17] or protein kinase B (AKT) signaling in hormone-dependent cancer models.[18]

Urease is a vital enzyme in plants that catalyzes the hydrolysis of urea into ammonia and carbon dioxide, allowing plants to access essential nitrogen for growth and protein synthesis.[19] It is critical for nitrogen recycling, seed germination, and defense mechanisms, while also enabling the uptake of urea-based fertilizers.[20,21] In the biomedical field, ureolytic activity represents a critical virulence factor for various pathogenic microorganisms.[22] Ureolytic bacteria possess the ability to catalyze the hydrolysis of urea, leading to the release of ammonia and a subsequent increase in the pH of the surrounding environment. For instance, the elevation of gastric pH during *Helicobacter pylori* infections is closely linked to severe pathologies, such as gastritis, peptic ulcers, and gastric cancer.[20] Furthermore, this enzymatic activity is associated with serious urinary tract infections, particularly those caused by *Proteus mirabilis*. Within this framework, the development of novel urease inhibitors has emerged as a crucial strategy in the rational design of new antimicrobial agents.[20,23]

The present study reports the evaluation of chromenes and Chro-DHPM hybrids as bioactive urease inhibitors. This hypothesis was envisaged based on several previous reports of urease inhibitory activity dihydropyrimidinones. Braga *et al.*[24] identified three Biginelli adducts with inhibitory activity comparable to that of hydroxyurea, which was used as a positive control in the *in vitro* urease screening assays. Costa *et al.*[25] synthesized and evaluated the urease inhibitory activity of a series of Biginelli adducts derived from formylphenylboronic acids. The most potent derivative exhibited half-maximal inhibitory concentration (IC_{50}) value of 132 ± 12 μM and acted as a mixed-type inhibitor.

Although chromene derivatives have been less extensively studied than Biginelli adducts as urease inhibitors, few studies have yielded promising results. For instance, Sul *et al.*[26] demonstrated the potent inhibitory activity of 2-amino-3-cyano-4*H*-chromene derivatives, which also affected swarming motility, biofilm formation and disruption, and urease production in *Proteus mirabilis*.

Results and Discussion

The synthetic strategy for the preparation of hybrids considered the connection of two pharmacophores through the formation of a non-enolizable triazole linker achieved via Huisgen reaction[27] catalyzed by Cu^{I} catalyst, well known as CuAAC protocol (copper-catalyzed azide-alkyne cycloaddition reaction).[28,29] The chromene unity was envisaged as the alkyne component while de DHPM derivative was the azide fragment (Scheme 1).

Synthesis of chromene derivatives

For the preparation of chromene **1a** and oxy-propargyl chromenes **1b**,**1c** the MCR (multicomponent reaction) of dimedone, malononitrile and respective aldehydes in DES (deep eutectic solvent) based on choline chloride:urea (1:3) as an environmentally friendly solvent afforded the desired chromenes in good yields (Scheme 2).[30] This protocol was extensively discussed in a previous report.[17] The results are shown in Table 1.

The appearance of a singlet around 4.15 ppm confirms the presence of benzylic hydrogen and formation of desired products.[17] Compounds **1a-1c** were fully characterized by conventional spectroscopic technics, including high-resolution mass spectrometry (HRMS).

Synthesis of 6-azido-DHPMs

The 6-azido-DHPM **3a-3d** were obtained in two steps from the Biginelli-type adduct.[31] The reaction of intermediate 6-chloro-DHPM **2a-2d** with sodium azide affords desired product in reasonable to good overall yields (Scheme 3).[31] The results are shown in Table 2.

All compounds were characterized by the usual ^{1}H and ^{13}C nuclear magnetic resonance (NMR) spectroscopy. The observation of two doublets around 4.34-4.48 ppm referent

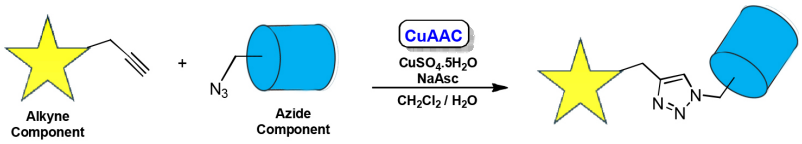

Scheme 1. Synthetic strategy for preparation of Chro-DHPM hybrids.

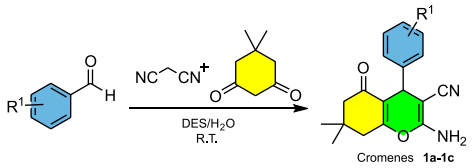

Scheme 2. Preparation of chromenes.

Table 1. Molecular structure of chromenes **1a-1c**

entry	Compound	Yield / %
1	**1a**	89
2	**1b**	88
3	**1c**	85

to diastereotopic hydrogens at C6 position and signal of the benzylic hydrogen around 5.20 ppm confirms the formation of products.[17]

Synthesis of hybrids chromene-DHPMs

With compounds **1b**,**1c** and **3a-3d** in hands, the CuAAC protocol was applied to connect the two unities with formation of a non-hydrolysable triazole ring as linker (Scheme 4). Thus, the chromene-DHPM hybrids (Chro-DHPM) **4a-4h** were obtained in reasonable to good yields. The results are shown in Table 3.

Table 2. Molecular structures of 6-azido-DHPMs **3a-3d**

entry	Compound	Yield / %
1	**3a**	68
2	**3b**	71
3	**3c**	76
4	**3d**	74

The appearance of a singlet around 7.85 ppm assigned as the triazole hydrogen, confirms the formation of the triazole linker and consequently, the connection of two unities.

In vitro antiureolytic activity

The antiureolytic activity was evaluated using the indophenol method, employing *Canavalia ensiformis* urease and urea as the substrate. A detailed description of the experimental procedures is provided in the Experimental section. Initially, the chromene-DHPM hybrids **4a-4h** were screened at a concentration of 100 μM to identify the most effective inhibitors. Thiourea (TIO) was used as the

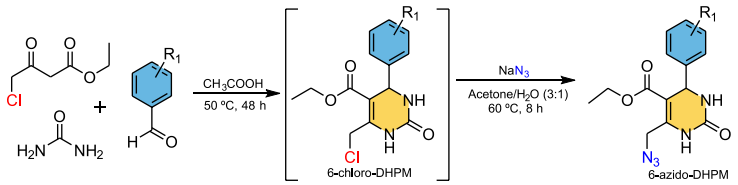

Scheme 3. Synthesis of 6-azido-DHPMs **3a-3d**.

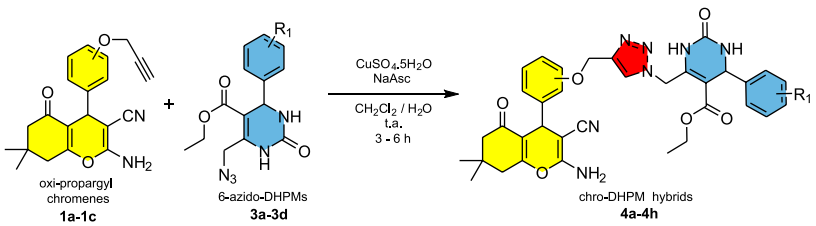

Scheme 4. Synthesis of chromene-DHPM hybrids **4a-4h**.

Table 3. Molecular structures of hybrid compounds **4a-4h**

entry		Hybrid Chro-DHPM	Yield / %
1	**4a**	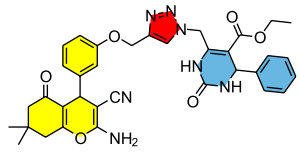	82
2	**4b**	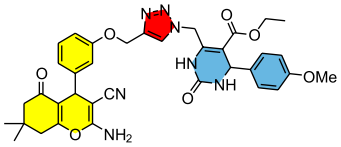	81
3	**4c**	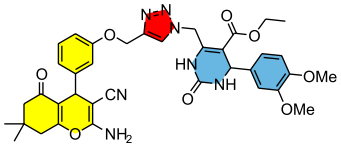	85
4	**4d**	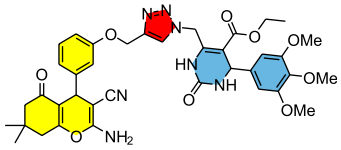	91
5	**4e**	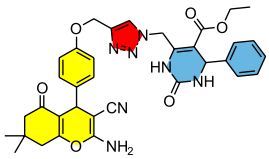	79
6	**4f**	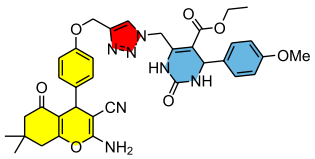	80
7	**4g**	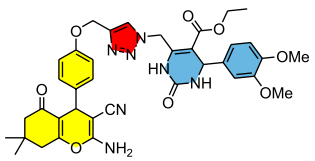	74
8	**4h**	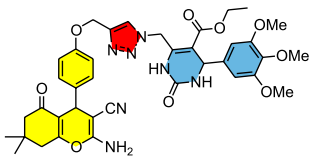	81

Chro-DHPM: chromene-dihydropyrimidinone.

reference standard under the same experimental conditions, due to its well-stablished role as urease inhibitor. The literature reports TIO as classic competitive inhibitor that effectively mimics the urea substrate, providing standardized reference for assessing the inhibitory efficacy of new synthetic inhibitors.[32-34] The results (Figure 1) revealed that hybrids **4b** and **4h** were the most potent, exhibiting 42.1 and 51.5% inhibition, respectively.

A preliminary structure-activity relationship (SAR) analysis suggests that the substitution pattern on DHPM scaffolds plays a crucial role in the inhibitory potency. The presence of electron-donating methoxyl groups appears to be a key factor for enhanced activity. Hybrid **4h**, bearing a 3,4,5-trimethoxyphenyl scaffold, emerged as the most potent inhibitor of the series (51.5% inhibition). Furthermore, the regiochemistry of the triazole linker on the aromatic ring of the DHPM moiety was relevant in the antiureolytic activity. Hybrid **4h** featuring the triazole bridge at the *para*-position displayed superior inhibitory profiles compared to their *ortho*-linked counterparts (**4d**).

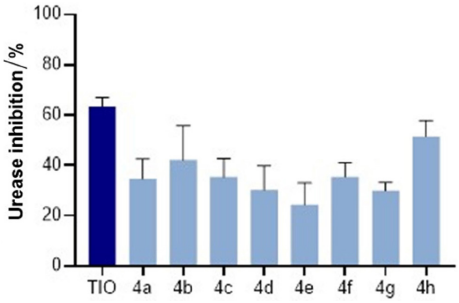

Figure 1. Effect of chromene-DHPM hybrids on the activity of type III urease from *Canavalia ensiformis*. Reactions contained 12.5 mU urease, 20 mM urea, and each compound test at 100 µM.

To investigate whether molecular hybridization enhances biological performance, the urease inhibitory activities of **4b** and **4h** were compared to those of their precursors, chromene (**1a**) and Biginelli adducts (**3b** and **3d**) (Figure 2).

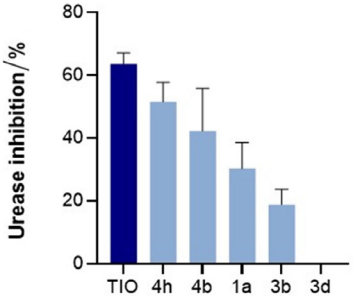

Figure 2. Effect of compounds **1a**, **3b**, **3d**, **4b** and **4h**, on the activity of type III urease from *Canavalia ensiformis*. Reactions contained 12.5 mU urease, 20 mM urea, and each compound test at 100 µM.

The Biginelli adduct **3b** showed low inhibitory activity (18.8%), while derivative **3d** was inactive at the tested concentration. Although chromene **1a** displayed superior activity (30.3%) compared to the Biginelli adducts, its potency remained lower than that of the hybrids. The molecular hybridization strategy proved to be an interesting approach in the search for novel antiureolytic agents. The significant increase in the inhibitory activity of

hybrids **4b** and **4h** compared to their precursors confirms the synergistic effect between the chromene and DHPM scaffolds. The linkage of the functionalized DHPM to the chromene scaffold via the triazole bridge likely provides the necessary conformational orientation for the DHPM carbonyl to coordinate with the binuclear nickel center, while the aromatic ring occupies auxiliary pockets. While the precise binding mode remains to be fully elucidated, it is plausible that the hybrid architecture allows for a more comprehensive occupation of the catalytic site, potentially targeting both the nickel center and the surrounding hydrophobic residues.

Molecular modeling

Initially, a comparative Ramachandran analysis between the native urease and the ligand-bound system revealed no significant differences in the stereochemical quality of the protein after molecular dynamics (MD) simulation. The native structure presented 81.5% of residues in the most favored regions, 17.0% in additionally allowed regions, and 1.4% in disallowed regions (Figure S17a, Supplementary Information (SI) section), whereas the complex with compound **4h** exhibited 82.7, 16.0, and 1.3%, respectively (Figure S17b, SI section). These closely comparable distributions indicate that the presence of the ligand does not induce structural destabilization, global unfolding, or significant conformational distortions in the enzyme. Instead, the overall folding and backbone geometry remain well preserved throughout the simulation, supporting the structural integrity of the catalytic machinery under ligand-bound conditions. Thus, the inhibitory profile of compound **4h** is unlikely to arise from nonspecific protein destabilization, but rather from localized interactions within the enzyme. In this context, a detailed analysis of the ligand-enzyme interactions at the catalytic site were conducted to elucidate the molecular basis of inhibition.

A detailed analysis of the MD simulations provided important insights into the binding behavior of compound **4h** within the urease active site. The most representative conformation from the MD trajectory showed that the carbonyl oxygen of the tetrahydropyrimidine moiety coordinates to the binuclear Ni^{2+} center, indicating that this functional group plays a key role in anchoring the ligand within the catalytic environment (Figure 3a).

Notably, the ligand adopts a partially inserted conformation, in which the tetrahydropyrimidine core is positioned within the catalytic cavity, while the tetrahydro-4*H*-chromene moiety remains oriented toward the entrance of the active site (Figure 3b).

This asymmetric positioning suggests that, in addition

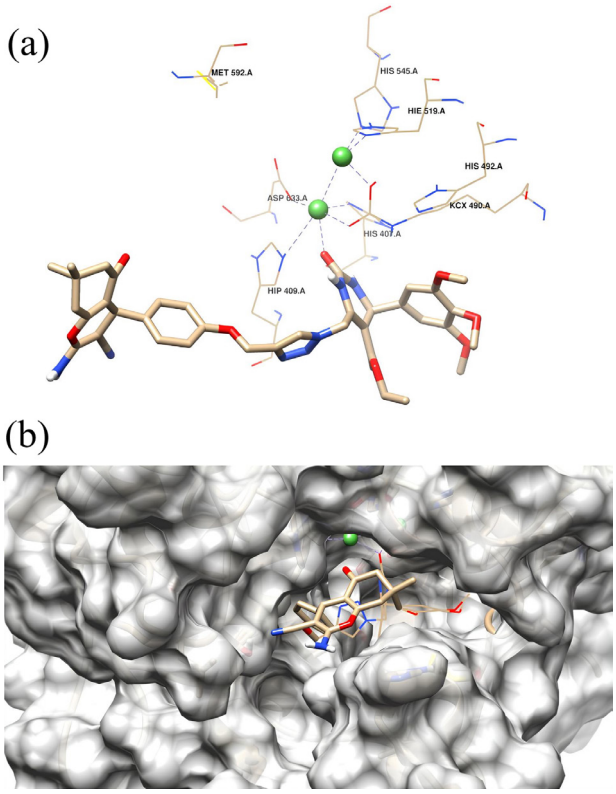

Figure 3. (a) 3D representation of interactions between **4h** with urease. The binding conformation of the ligand is visualized using a stick representation, while green spheres denote the two Ni metals. The coordination with metal, hydrogen bonding, and ionic interactions are illustrated using dotted lines. (b) A schematic allosteric and catalytic sites representation for the most representative conformation of the complex for **4i**. The binding conformation of the ligand is visualized using a stick representation, while green spheres denote the two Ni metals.

to metal coordination, steric effects may contribute significantly to the inhibitory mechanism. In this context, the ligand appears to simultaneously interact with the catalytic center and obstruct substrate access, supporting a hybrid inhibition model.

The root mean square deviation (RMSD) analysis provides further support for this binding behavior. The trajectory indicates that compound **4h** undergoes a progressive insertion process, entering the catalytic site within the first ca. 30 ns of simulation, followed by a stabilization phase around 50 ns. After this equilibration period, the complex remains stable throughout the remainder of the simulation. Following equilibration, RMSD values fluctuated between 0.6 and 1.2 Å for the ligand and between 1.8 and 3.0 Å for the protein Cα atoms, indicating that both the ligand and the protein maintain structural stability under the simulated conditions (Figure 4a).

Throughout the MD trajectory, the **4h**-urease complex remained stabilized by interactions with key catalytic residues, including His407, His409, KCX490, and

Asp633. These residues predominantly formed hydrogen bonds and ionic interactions that persisted throughout the simulation, indicating persistent ligand anchoring within the catalytic region. Importantly, although coordination with the Ni^{2+} center is observed, the overall interaction profile is not restricted to classical deep binding within the active site. Instead, stabilization arises from a combination of metal coordination and extended interactions at the catalytic entrance (Figure 4b). These results suggest that compound **4h** does not follow a purely classical competitive inhibition mechanism. Rather, the observed binding mode supports a hybrid model in which partial insertion into the catalytic cavity, combined with steric hindrance at the active site entrance, contributes to enzyme inhibition.

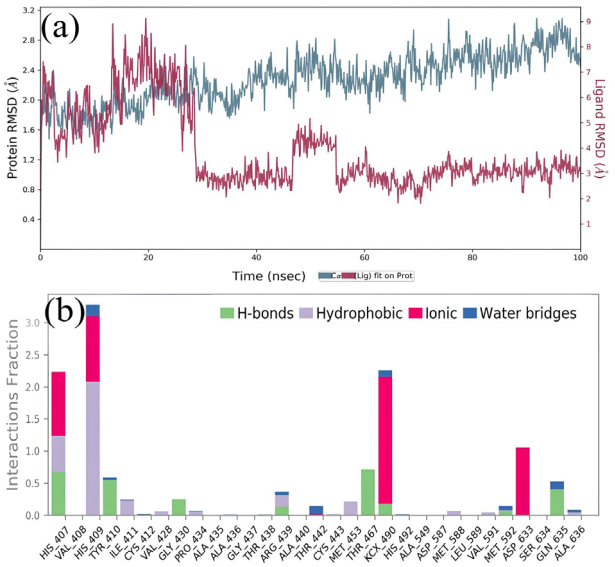

Figure 4. (a) Protein interactions with the inhibitor **4h** were monitored throughout the MD simulation. A value of 1.0 suggests that the specific interaction is sustained throughout 100% of the simulation, while values over 1.0 arise when the residue establishes numerous contacts of the identical subtype with the ligand. (b) RMSD plots of the urease backbone and ligands **4h** within the target.

Conclusions

In conclusion, the molecular hybridization of chromene and DHPM scaffolds proved to be a successful strategy, yielding novel compounds (e.g., **4b** and **4h**) with significantly enhanced urease inhibitory activity compared to their individual precursor units. This synergistic effect confirms the potential of hybrid architecture to more effectively target the active site of the enzyme, providing a promising foundation for the development of new antiureolytic agents. MD simulations demonstrated that the most active derivative **4h** can coordinate with the binuclear Ni^{2+} center through the carbonyl oxygen of the tetrahydropyrimidine moiety, while adopting a partially inserted conformation within the active site. This binding mode reveals that effective inhibition is not necessarily dependent on complete accommodation within the catalytic cavity. Instead, compound **4h** exhibits a hybrid inhibition mechanism, combining catalytic site interaction with steric obstruction at the entrance of the binding pocket. This dual behavior allows the ligand to remain stably associated with the enzyme while potentially restricting substrate access.

Experimental

Chemistry

The reagents were purchased from commercial sources and used without further purification, except ethyl acetate and hexanes, which were purified by simple distillation. Column chromatography was performed using a Silica Gel 60 Å (ACROS Organics, 0.035-0.070 mm). The reactions were monitored using thin-layer chromatography (TLC) and visualized under UV light. The NMR spectra were recorded using Varian VNMRS 300 spectrometer (^{1}H at 300 MHz and ^{13}C at 75 MHz) or Bruker (^{1}H at 400 MHz and ^{13}C at 100 MHz in dimethyl sulfoxide (DMSO-d_6) as solvent). The chemical shifts (δ) are reported in ppm units downfield from DMSO δ = 2.50 ppm for ^{1}H NMR, and δ = 39.5 for the ^{13}C NMR. The coupling constants (J) are reported in Hz and refer to peak multiplicities, which are described as s for singlet, bs for broad singlet, d for doublet, t for triplet, dd for doublet of doublets, ddd for doublet of doublets of doublets, dt for doublet of triplets, and m for multiplet. The HRMS were obtained on a Bruker Impact II (ESI-QTOF-MS) in positive electrospray ionization (ESI) mode using DMSO as solvent. All compounds were purified by silica gel column chromatography (230-400 mesh) prior to NMR and HRMS analysis.

General procedure for the synthesis of hybrids **4a-4h**

In a dry 25 mL round-bottom flask equipped with a magnetic stirrer, 0.3 mmol of azido dihydropyrimidinone (**3a-3d**) was added, followed by 3 mL of dichloromethane, 3 mL of water, 0.3 mmol of oxi-propargyl chromenes (**1c**,**1b**), 0.06 mmol (11.9 mg) of sodium ascorbate and 0.03 mmol (7.5 mg) of $CuSO_4.5H_2O$. The mixture was kept at room temperature (25 ºC) under stirring and monitored by TLC (ethyl acetate 70% in hexane or ethyl acetate). After the consumption of one limiting reagent, 6 mL of 0.1 mol L^{-1} of ethylenediaminetetraacetic acid (EDTA) aqueous solution was added and the mixture

was stirred for more than 5 min. Then, the biphasic solution was extracted with dichloromethane (4 × 5 mL) and the solvent was removed under vacuum. All the crude products were purified by silica column chromatography before the spectroscopic analysis.

Ethyl 6-((4-((3-(2-amino-3-cyano-7,7-dimethyl-5-*oxo*-5,6,7,8-tetrahydro-4*H*-chromen-4-yl)phe noxy)methyl)-1*H*-1,2,3-triazol-1-yl)-methyl)-2-*oxo*-4-phenyl-1,2,3,4-tetrahydropyrimidine-5-carboxy late (**4a**)

Pale yellow solid; ^{1}H NMR (400 MHz, DMSO-d_6) δ 9.60 (1H, bs), 8.21 (1H, s), 7.89 (1H, bs), 7.35-2.27 (5H, m), 7.22 (1H, t, *J* 8.2 Hz), 7.01 (2H, bs), 6.92-6.90 (1H, m), 6.76-6.74 (2H, m), 5.70 (1H, d, *J* 13.9 Hz), 5.49-5.45 (1H, m), 5.23 (1H, d, *J* 3.2 Hz), 5.14 (1H, d, *J* 11.8 Hz), 5.09 (1H, d, *J* 11.8 Hz), 4.16 (1H, s), 4.01 (2H, q, *J* 7.1 Hz), 2.58-2.47 (2H, m + DMSO), 2.24 (1H, d, *J* 16.0 Hz), 2.13 (1H, d, *J* 15.9 Hz), 1.07-1.03 (6H, m), 0.97 (3H, s); ^{13}C NMR (100 MHz, DMSO-d_6) δ 196.2, 165.0, 163.1, 159.0, 158.6, 152.2, 146.9, 144.4, 143.6, 142.8, 129.9, 129.0, 128.1, 126.9, 125.6, 120.3, 120.2, 114.5, 113.0, 112.5, 103.4, 61.4, 60.5, 58.7, 54.6, 50.5, 48.4, 35.9, 32.3, 28.7, 27.5, 14.3; HRMS (ESI) *m/z*, calcd. for $[C_{35}H_{36}N_7O_6 + H]^+$: 650.2722, found: 650.2724.

Ethyl 6-((4-((3-(2-amino-3-cyano-7,7-dimethyl-5-*oxo*-5,6,7,8-tetrahydro-4*H*-chromen-4-yl)phe noxy)methyl)-1*H*-1,2,3-triazol-1-yl)methyl)-4-(4-methoxyphenyl)-2-*oxo*-1,2,3,4-tetrahydropy rimidine-5-carboxylate (**4b**)

Pale yellow solid; ^{1}H NMR (400 MHz, DMSO-d_6) δ 9.54 (1H, bs), 8.21 (1H, s), 7.82-7.81 (1H, m), 7.24-7.18 (3H, m), 7.00 (2H, bs), 6.92-6.86 (3H, m), 6.76-6.74 (2H, m), 5.69 (1H, d, *J* 14.0 Hz), 5.47 (1H, dd, *J* 14.0 and 2.5 Hz), 5.18 (1H, d, *J* 3.2 Hz), 5.14 (1H, d, *J* 12.0 Hz), 5.09 (1H, d, *J* 11.8 Hz), 4.16 (1H, s), 4.01 (2H, q, *J* 7.1 Hz), 3.72 (3H, s), 2.58-2.47 (2H, m + DMSO), 2.24 (1H, d, *J* 16.0 Hz), 2.14 (1H, d, *J* 15.9 Hz), 1.09-1.03 (6H, m), 0.97 (3H, s); ^{13}C NMR (100 MHz, DMSO-d_6) δ 195.8, 164.6, 162.7, 158.7, 158.6, 158.1, 151.8, 146.5, 142.8, 142.3, 136.1, 129.5, 127.7, 125.2, 119.8, 119.8, 114.0, 113.8, 112.6, 112.1, 103.3, 60.9, 60.0, 58.2, 55.1, 53.6, 50.0, 48.0, 35.5, 31.9, 28.3, 27.0, 13.9; HRMS (ESI) *m/z*, calcd. for $[C_{36}H_{38}N_7O_7 + H]^+$: 680.2827, found: 680.2820.

Ethyl 6-((4-((3-(2-amino-3-cyano-7,7-dimethyl-5-*oxo*-5,6,7,8-tetrahydro-4*H*-chromen-4-yl)phe noxy)methyl)-1*H*-1,2,3-triazol-1-yl)-methyl)-4-(3,4-dimethoxyphenyl)-2-*oxo*-1,2,3,4-tetrahydro pyrimidine-5-carboxylate (**4c**)

Pale yellow solid; ^{1}H NMR (400 MHz, DMSO-d_6) δ 9.55 (1H, bs), 8.23 (1H, s), 7.81 (1H, bs), 7.22 (1H, t, *J* 8.2 Hz), 7.00 (2H, bs), 6.92-6.86 (3H, m), 6.79-6.74 (3H, m), 5.67-5.63 (1H, m), 5.55-5.51 (1H, m), 5.18 (1H, d, *J* 3.2 Hz), 5.14 (1H, d, *J* 11.8 Hz), 5.09 (1H, d, *J* 11.8 Hz), 4.16 (1H, s), 4.06–3.95 (2H, m), 3.72 (3H, s), 3.70 (3H, s), 2.58-2.47 (2H, m + DMSO), 2.24 (1H, d, *J* 16.1 Hz), 2.13 (1H, d, *J* 16.1 Hz), 1.07 (3H, t, *J* 7.1 Hz), 1.03 (3H, s), 0.97 (3H, s); ^{13}C NMR (100 MHz, DMSO-d_6) δ 195.7, 164.5, 162.6, 158.5, 158.1, 151.8, 148.7, 148.2, 146.4, 143.0, 142.3, 136.4, 129.4, 125.3, 119.8, 119.7, 118.4, 114.0, 112.6, 112.1, 111.6, 110.1, 102.8, 60.9, 60.0, 58.2, 55.5, 55.4, 53.8, 50.0, 48.1, 35.4, 31.8, 28.3, 27.0, 13.9; HRMS (ESI) *m/z*, calcd. for $[C_{37}H_{40}N_7O_8 + H]^+$: 710.2933, found: 710.2923.

Ethyl 6-((4-((3-(2-amino-3-cyano-7,7-dimethyl-5-*oxo*-5,6,7,8-tetrahydro-4*H*-chromen-4-yl)phe noxy)methyl)-1*H*-1,2,3-triazol-1-yl)-methyl)-2-*oxo*-4-(3,4,5-trimethoxyphenyl)-1,2,3,4-tetrahy dropyrimidine-5-carboxylate (**4d**)

Pale yellow solid; ^{1}H NMR (400 MHz, DMSO-d_6) δ 9.60 (1H, bs), 8.26 (1H, s), 7.83 (1H, bs), 7.21 (1H, t, *J* 7.9 Hz), 7.00 (2H, bs), 6.89 (1H, d, *J* 8.1 Hz), 6.74-6.72 (2H, m), 6.55 (2H, s), 5.84-5.80 (1H, m), 5.34 (1H, d, *J* 14.0 Hz), 5.17 (1H, d, *J* 2.8 Hz), 5.12 (1H, d, *J* 11.8 Hz), 5.06 (1H, d, *J* 11.8 Hz), 5.14 (1H, s), 4.00 (2H, q, *J* 7.1 Hz), 3.70 (6H, s), 3.61 (3H, s), 2.56-2.46 (2H, m + DMSO), 2.23 (1H, d, *J* 16.1 Hz), 2.11 (1H, d, *J* 16.0 Hz), 1.06-1.01 (6H, m), 0.95 (3H, s); ^{13}C NMR (100 MHz, DMSO-d_6) δ 195.7, 164.5, 162.6, 158.5, 158.1, 152.9, 151.7, 146.4, 143.5, 142.3, 139.4, 136.8, 129.4, 125.4, 119.8, 119.7, 114.0, 112.6, 112.1, 103.6, 102.2, 60.9, 60.0, 60.0, 58.2, 55.8, 54.2, 50.0, 48.2, 35.4, 31.8, 28.3, 26.9, 13.9; HRMS (ESI) *m/z*, calcd. for $[C_{38}H_{42}N_7O_9 + H]^+$: 740.3039, found: 740.3028.

Ethyl 6-((4-((4-(2-amino-3-cyano-7,7-dimethyl-5-*oxo*-5,6,7,8-tetrahydro-4*H*-chromen-4-yl)phe noxy)methyl)-1*H*-1,2,3-triazol-1-yl)-methyl)-2-*oxo*-4-phenyl-1,2,3,4-tetrahydropyrimidine-5-carboxylate (**4e**)

Pale yellow solid; ^{1}H NMR (400 MHz, DMSO-d_6) δ 9.60 (1H, bs), 8.19 (1H, s), 7.90 (1H, bs), 7.35-7.25 (5H, m), 7.07 (2H, d, *J* 8.7 Hz), 6.98 (2H, bs), 6.95 (2H, d, *J* 8.7 Hz), 5.69 (1H, d, *J* 13.9 Hz), 5.47 (1H, d, *J* 13.9 Hz), 5.22 (1H, d, *J* 3.2 Hz), 5.11 (2H, bs), 4.13 (1H, s), 4.00 (2H, q, *J* 7.1 Hz), 3.35 (1H, s), 2.55-2.46 (2H, m + DMSO), 2.25 (1H, d, *J* 16.1 Hz), 2.10 (1H, d, *J* 16.0 Hz), 1.07-1.03 (6H, m), 0.95 (3H, s); ^{13}C NMR (100 MHz, DMSO-d_6) δ 195.7, 164.5, 162.2, 158.5, 156.8, 151.8, 143.9, 143.1, 142.5, 137.2, 128.5, 128.3, 127.6 126.5, 125.0, 119.9, 114.4, 113.0, 103.0, 60.9, 60.1, 58.5, 54.2, 50.0, 48.0, 34.8, 31.8, 28.4, 26.8, 13.8; HRMS (ESI) calcd. for $[C_{35}H_{36}N_7O_6 + H]^+$: 650.2722, found: 650.2714.

Ethyl 6-((4-((4-(2-amino-3-cyano-7,7-dimethyl-5-*oxo*-5,6,7,8-tetrahydro-4*H*-chromen-4-yl)phe noxy)methyl)-1*H*-1,2,3-triazol-1-yl)methyl)-4-(4-methoxyphenyl)-2-*oxo*-1,2,3,4-tetrahydropyri midine-5-carboxylate (**4f**)

Pale yellow solid; ^{1}H NMR (400 MHz, DMSO-d_6) δ 9.56 (1H, bs), 8.18 (1H, s), 7.83 (1H, bs), 7.19 (2H, d, *J* 8.7 Hz), 7.07 (2H, d, *J* 8.8 Hz), 6.98 (2H, bs), 6.96 (2H, d, *J* 8.8 Hz), 6.88 (2H, d, *J* 8.8 Hz), 5.68 (1H, d, *J* 13.9 Hz), 5.47 (1H, d, *J* 13.9 Hz), 5.17 (1H, d, *J* 3.1 Hz), 5.11 (2H, bs), 4.13 (1H, s), 4.00 (2H, q, *J* 7.1 Hz), 3.72 (3H, s), 2.55-2.45 (2H, m + DMSO), 2.25 (1H, d, *J* 16.1 Hz), 2.10 (1H, d, *J* 16.1 Hz), 1.06 (3H, t, *J* 7.1 Hz), 1.03 (3H, s), 0.95 (3H, s); ^{13}C NMR (100 MHz, DMSO-d_6) δ 195.7, 164.5, 162.2, 158.7, 158.4, 156.8, 151.8, 142.7, 142.5, 137.2, 136.1, 128.2, 127.6, 124.9, 119.8, 114.4, 113.8, 113.0, 103.3, 61.0, 60.0, 59.0, 55.1, 54.0, 50.0, 48.0, 34.7, 31.8, 28.4, 26.8, 13.8; HRMS (ESI) *m/z*, calcd. for $[C_{36}H_{38}N_7O_7 + H]^+$: 680.2827, found: 680.2819.

Ethyl 6-((4-((4-(2-amino-3-cyano-7,7-dimethyl-5-*oxo*-5,6,7,8-tetrahydro-4*H*-chromen-4-yl)phe noxy)methyl)-1*H*-1,2,3-triazol-1-yl)methyl)-4-(3,4-dimethoxyphenyl)-2-*oxo*-1,2,3,4-tetrahydro pyrimidine-5-carboxylate (4g)

Pale yellow solid; ^{1}H NMR (400 MHz, DMSO-d_6) δ 9.57 (1H, bs), 8.20 (1H, s), 7.82 (1H, bs), 7.06 (2H, d, *J* 8.6 Hz), 6.98 (2H, sl), 6.95 (2H, d, *J* 8.6 Hz), 6.88 (1H, d, *J* 8.3 Hz), 6.85 (1H, d, *J* 1.7 Hz), 6.77 (1H, dd, *J* 8.3 and 1.5 Hz), 5.65 (1H, d, *J* 13.9 Hz), 5.51 (1H, d, *J* 13.8 Hz), 5.17 (1H, d, *J* 2.9 Hz), 5.11 (2H, bs), 4.13 (1H, s), 4.00 (2H, q, *J* 6.8 Hz), 3.71 (3H, s), 3.69 (3H, s), 2.55-2.45 (2H, m + DMSO), 2.24 (1H, d, *J* 16.1 Hz), 2.10 (1H, d, *J* 16.1 Hz), 1.08-1.03 (6H, m), 0.95 (3H, s); ^{13}C NMR (100 MHz, DMSO-d_6) δ 195.7, 164.5, 162.2, 158.5, 156.8, 151.8, 148.7, 148.3, 143.0, 142.5, 137.2, 136.4, 128.3, 125.1, 119.8, 118.5, 114.4, 113.0, 111.6, 110.1, 102.9, 61.0, 60.0, 58.5, 55.5, 55.4, 53.8, 50.0, 48.1, 34.8, 31.8, 28.4, 26.8, 13.9; HRMS (ESI) *m/z*, calcd. for $[C_{37}H_{40}N_7O_8 + H]^+$: 710.2933, found: 710.2933.

Ethyl 6-((4-((4-(2-amino-3-cyano-7,7-dimethyl-5-*oxo*-5,6,7,8-tetrahydro-4*H*-chromen-4-yl)phe noxy)methyl)-1*H*-1,2,3-triazol-1-yl)methyl)-2-*oxo*-4-(3,4,5-trimethoxyphenyl)-1,2,3,4-tetrahy dropyrimidine-5-carboxylate (**4h**)

Pale yellow solid; ^{1}H NMR (400 MHz, DMSO-d_6) δ 9.60 (1H, bs), 8.24 (1H, s), 7.83 (1H, bs), 7.07 (2H, d, *J* 8.6 Hz), 6.96-6.94 (4H, m), 6.56 (2H, s), 5.83 (1H, d, *J* 14.0 Hz), 5.36 (1H, d, *J* 13.9 Hz), 5.18 (1H, d, *J* 3.2 Hz), 5.11 (2H, sl), 4.14 (1H, s), 4.01 (2H, q, *J* 7.2 Hz), 3.71 (6H, s), 3.62 (3H, s), 2.55-2.45 (2H, m + DMSO), 2.25 (1H, d, *J* 16.0 Hz), 2.10 (1H, d, *J* 16.1 Hz), 1.07-1.03 (6H, m), 0.95 (3H, s); ^{13}C NMR (100 MHz, DMSO-d_6) δ 195.7, 164.5, 162.2, 158.5, 156.8, 152.9, 151.7, 143.5, 142.5, 139.5, 137.2, 136.8, 128.3, 125.3, 119.8, 114.4, 113.0, 103.5, 102.2, 60.9, 60.0, 60.0, 58.5, 55.8, 54.2, 50.0, 48.2, 34.8, 31.8, 28.4, 26.8, 13.9; HRMS (ESI) *m/z*, calcd. for $[C_{38}H_{42}N_7O_9 + H]^+$: 740.3039, found: 740.3027.

In vitro antiureolytic activity

Urease inhibition was assessed using the Berthelot method,[35] which quantifies ammonium ions through the creation of indophenol, a vivid blue compound. The assays were performed in ELISA microplates by mixing 10 µL of an ethanolic solution of the test compounds, 80 µL of urease solution (2.5 U mL^{-1} in phosphate buffer, pH 7.0), and 10 µL of urea aqueous solution (100 mM). After an initial incubation at 25 °C for 10 min (600 rpm), the reaction was treated with 45 µL of solution A (1% phenol/0.005% sodium nitroprusside) and 70 µL of solution B (0.5% NaOH/0.1% sodium hypochlorite). A second incubation followed at 50 °C for 5 min (600 rpm), and the absorbance was measured at 630 nm to calculate the percentage of inhibition.

Molecular modeling

The *in silico* simulations were performed using the co-crystallized structure of jack bean urease (PDB entry: 4H9M), obtained from the Research Collaboratory for Structural Bioinformatics Protein Data Bank (RCSB PDB).[36] Initially, the native conformation of the target protein was refined through preliminary MD simulations, and the most stable structure was selected for subsequent analyses. Trajectory analyses included RMSD, root mean square fluctuation (RMSF), and monitoring of ligand-protein interactions throughout the simulation. The structural integrity of the system was assessed by Ramachandran plot analysis, which was generated both before and after MD simulations of the ligand-urease complex using the SAVES v6.0 server.[37] All MD parameters and system preparation protocols were employed as previously described by our research group,[38-40] ensuring methodological consistency and reproducibility, and therefore are not described in detail herein.

Molecular modeling studies were conducted to investigate the binding mode of the most active derivative **4h** within the urease active site. Although conventional molecular docking protocols were initially considered, preliminary structural inspection revealed a steric mismatch between the ligand size and the geometry of the catalytic cavity. This observation, combined with the conformational flexibility of the ligand, indicated potential limitations in the application of standard docking approaches for reliable pose prediction.

It is well established that molecular docking methods may exhibit reduced accuracy when applied to bulky and highly flexible ligands, mainly due to restricted conformational sampling and the use of simplified scoring functions.[41] In addition, most docking protocols treat the receptor as rigid, neglecting protein flexibility and induced-fit effects, which are critical for ligand accommodation in enzymatic systems.[42] These limitations are particularly relevant in metalloenzymes such as urease, where structural rearrangements of the active site may play an important role during ligand binding. Considering these limitations, an alternative MD-based strategy was employed. Instead of relying on docking-derived poses, compound **4h** was initially positioned at the entrance of the catalytic pocket, allowing the system to evolve dynamically during the simulation. This approach enables the exploration of ligand binding pathways and protein flexibility, which are not adequately captured by conventional docking methodologies.[43,44]

Supplementary Information

Supplementary information of ^{1}H NMR, ^{13}C NMR spectra of hybrid compounds **4a**-**4h**; figures of Ramachandran plot analysis and table of urease inhibition's values from *Canavalia ensiformis* are available free of charge at http://jbcs.sbq.org.br as PDF file.

Data Availability Statement

The data supporting this article is available in the text.

Acknowledgments

We dedicate this work to Prof Dr Ronaldo Aloise Pilli in celebration of his 70th birthday and his retirement from the academic services at Universidade Estadual de Campinas/SP, Brazil. His outstanding contributions to Chemistry science, unwavering commitment to academic excellence, and lasting impact on students and colleagues have profoundly shaped the field of Organic Synthesis in Brazil. We express our deepest gratitude and wish him continued fulfillment and success in this new chapter.

The authors are grateful to the governmental agencies for financial support and fellowships. FAPERGS (D. R. grant No. 19/2551-0001767-7); CNPq (D. R. grant No. 310438/2020-9 and 403260/2021-3). CAPES for the fellowship (S. J. S.). CNPq (A. F. grant No. 305175/2018-1 and 408590/2021-1), CAPES (A.F. grant No. Financial code 001 and 23038.000273/2025-99) and FAPEMIG (A. F. grant No RED-00082-23 (process 69206) and BPD-00390-22). This work was also made possible, partly, by the National Institute of Science and Technology (INCT) on Urease Inhibitors of Agricultural and Medicinal Interest and the Network of Biostimulants and Increased Efficiency Fertilizers (CNPq, grant No. 406744/2022-0, FAPEMIG, grants No. RED-00082-23 and APQ-04111-24, and CAPES, grants No. 88887.954439/2024-00)

The authors have used the ChatGPT (GPT-5, OpenAI, August 2025) and Gemini 2.5 Flash (Google, February 2026) to assist with language editing, including grammar stylistic refinements and modification of original figure used as Graphical Abstract. All content was revised by the authors, who take full responsibility for the final version and its scientific integrity.

Author Contributions

S. J. S.: synthesis, data acquisition and analysis, methodology, investigation. L. P. S. V.: writing, data acquisition and analysis, methodology, investigation. Y. S. C.: biological assays, investigation, methodology. N. M.L. F.: molecular modeling studies, data acquisition and analysis. T. M. A., Â. de F. and D. R.: writing, conceptualization, supervision, resources, funding acquisition.

References

1. Viegas-Junior, C.; Danuello, A.; Bolzani, V. S.; Barreiro, E. J.; Fraga, C. A.; *Curr. Med. Chem.* **2007**, *14*, 1829. [Crossref]
2. Meunier B.; *Acc. Chem. Res.* **2008**, *41*, 69. [Crossref]
3. Ivasiv, V.; Albertini, C.; Gonçalves, A. E.; Rossi, M.; Bolognesi, M. L.; *Curr. Top. Med. Chem.* **2019**, *19*, 1694. [Crossref]
4. Hansika, B. L. S.; Kamala, G. R.; Charishma, S.; *J. Pharma Insights Res.* **2025**, 3, 86. [Crossref]
5. Morphy, R.; Rankovic, Z.; *J. Med. Chem.* **2005**, *48*, 6523. [Crossref]
6. Bansal, Y.; Silakari, O.; *Eur. J. Med. Chem.* **2014**, *76*, 31. [Crossref]
7. Zimmermann, G. R.; Lehár, J.; Keith, C. T.; *Drug Discovery Today* **2007**, *12*, 34. [Crossref]
8. Bérubé, G.; *Expert. Opin. Drug Discovery* **2016**, *11*, 281. [Crossref]
9. Shaveta; Mishra, S.; Singh, P.; *Eur. J. Med. Chem.* **2016**, *124*, 500. [Crossref]
10. Alkhzem, A. H.; Woodman, T. J.; Blagbrough, I. S.; *RSC Adv.* **2022**, *12*, 19470. [Crossref]
11. Vendrusculo, V.; Souza, V. P.; Fontoura, L. A. M.; D'Oca, M. G. M.; Banzato, T. P.; Monteiro, P. A.; Pilli, R. A.; Carvalho, J. E.; Russowsky, D.; *Med. Chem. Commun.* **2018**, *9*, 1553. [Crossref]
12. Treptow, T. G. M.; Figueiró, F.; Jandrey, E. H. F.; Battastini, A. M. O.; Salbego, C. G.; Hoppe, J. B.; Taborda, P. S.; Rosa, S. B.; Piovesan. L. A.; D'Oca, C. R. M.; Russowsky, D.; D'Oca, M. G. M.; *Eur. J. Med. Chem.* **2015**, *95*, 552. [Crossref]
13. Souza, V. P.; Santos, F. S.; Rodembusch, F. S.; Braga, C. B.; Ornelas, C.; Pilli, R. A.; Russowsky, D.; *New J. Chem.* **2020**, *44*, 12440. [Crossref]

14. Souza, V. P.; Gomes, I. N. F.; Santos, S. J.; Braga, C. B.; Bezerra, A. J. A.; Philot, E. A.; Ramos, C. R. N.; Pantaleão, S. Q.; Silva, L. S.; Pilli, R. A.; Reis, R. M.; Oliveira, R. J. S.; Russowsky, D.; *RSC Med. Chem.* **2025**, *16*, 5989. [Crossref]
15. Vendrusculo, V.; Oliveira, M. P. L. S.; Rodrigues, B. A.; Ramos, V. S.; Menezes, J. M.; Zimmer, K. R.; Russowsky, D.; *ChemMedChem* **2025**, *20*, e202500716. [Crossref]
16. Paczkowski, I. M.; Guedes, E. P.; Mass, E. B.; Meneses, E. W.; Marques, Mantovani, M. S.; Russowsky, D.; *J. Heterocycl. Chem.* **2020**, *57*, 2597. [Crossref]
17. Santos, S. J.; Rossatto, F. C. P.; Jardim, N. S.; Ávila, D. S.; Ligabue-Braun, R.; Fontoura, L. A. M.; Zimmer, K. R.; Russowsky, D.; *New J. Chem.* **2023**, *47*, 7500. [Crossref]
18. Tejada, A. H.; Santos, S. J.; Lobo, G. T.; Ariwoola, A.-B. A.; Bezerra, A. J. A.; Stringhetta, G. R.; Gomes, I. N. F.; Silva, L. S.; Reis, R. M. V.; D'Almeida Preto, D.; Russowsky, D.; Silva-Oliveira, R. J.; *Pharmaceutics* **2025**, *17*, 1470. [Crossref]
19. Coelho, Y. S.; Silveira, A. J. B.; Oliveira, M. N.; Silva, P. G. S.; Pessoa, E. S.; Tolomeu, H. V.; Viana, L. P. S.; Enes, K. B.; da Silva, C. M.; Modolo, L. V.; de Fátima, Â.; *Quim. Nova* **2026**, *49*, e-20260048 [Crossref]; Horta, L. P.; Mota, Y. C. C.; Barbosa, G. M.; Braga, T. C.; Marriel, I. E.; de Fátima, Â.; Modolo, L. V.; *J. Braz. Chem. Soc.* **2016**, *8*, 1512 [Crossref]; Chaves-Silva, S.; Horta, L. P.; Souza, L. T.; da Silva, C. M.; Dohanik, C. S.; Goulart, G. A. C.; Marriel, I. E.; de Fátima, Â.; Modolo, L. V.; *Ind. Crops Prod.* **2020**, *145*, 111995. [Crossref]
20. Khan, M.; Zhang, B.; Zhang, H.; Wu, J.; Gao, P.; Li, J.; *Int. J. Biol. Macromol.* **2025**, *306*, 141702. [Crossrerf]
21. Ojha, A.; Bandyopadhyay, T. K.; Das, D.; *Critical Rev. Biotechnol.* **2026**, *46*, 1. [Crossref]
22. Rutherford, J. C.; *PLoS Pathog.* **2014**, *10*, e1004062. [Crossref]
23. Konieczna, I.; Zarnowiec, P.; Kwinkowski, M.; Kolesinska, B.; Fraczyk, J.; Kaminski, Z.; Kaca, W.; *Curr. Protein Pept. Sci.* **2012**, *13*, 789. [Crossref]
24. Braga, T. C.; Silva, T. F.; Maciel, T. M. S.; Silva, E. C. D.; Silva-Júnior, E. F.; Modolo, L. V.; Figueiredo, I. M.; Santos, J. C. C.; de Aquino, T. M.; de Fátima, Â.; *New J. Chem.* **2019**, *43*, 15187. [Crossref]
25. Costa, N. E. M.; Santos, P. H. C.; Medeiros, V. G. S.; Guimarães, A. S.; Santos, J. C. C.; Freire, N. M. L.; Silva. J. C. S.; Modolo, L.V.; Alberto, E. E.; de Fátima, Â.; *Bioorg. Chem.* **2024**, *152*, 107735. [Crossref]
26. Sul, R. D.; Humbe, O. Y.; Shelar, A, V.; Patil, R. H.; Khedkar, V. M.; Kale, B. B.; Nikam, L. K.; *ChemSelect* **2024**, *9*, e202304957. [Crossref]
27. Gonzaga, D. T. G.; Forezi, L. S. M.; Lima, C. G. S.; Ferreira, P. G.; da Silva, F. C.; Ferreira, V. S.; *Quim. Nova* **2025**, *44*, 235. [Crossref]
28. Kolb, H. C.; Finn, M. G.; Sharpless, K. B.; *Angew. Chem., Int. Ed.* **2001**, *40*, 2004. [Crossref]
29. Tornoe, C. W.; Christensen, C.; Meldal, M.; *J. Org. Chem.* **2002**, *67*, 3057. [Crossref]
30. Azizi, N.; Dezfooli, S.; Khajeh, M.; Hashemi, M. M.; *J. Mol. Liq.* **2013**, *186*, 76. [Crossref]
31. Lebed, P. S.; Kos, P. O.; Polovinko, V. V.; Tolmachev, A. A.; Vovk, M. V.; *Russ. J. Org. Chem.* **2009**, *45*, 921 [Crossref]; Chen, J.; Fu, X.; Zhou, L.; Zhang, J.; Qi, X.; Cao, X.; *J. Org. Chem.* **2009**, *74*, 4149. [Crossref]
32. Zahra, U.; Zaib, S.; Saeed, A.; Rehman, M.; Shabir, G.; Alsaab, H.; Khan, I.; *Inter. J. Biol. Macrom*. **2022**, *198*, 157. [Crossref]
33. Khan, K.; Naz, F.; Taha, M.; Khan, A.; Perveen, S.; Choudhary, M.; Voelter, W.; *Eur. J. Med. Chem*. **2014**, *74*, 314. [Crossref]
34. Mehmood, R.; Sadiq, A.; Alsantali, R.; Mughal, E.; Alsharif, M.; Naeem, N.; Javid, A.; Al-Rooqi, M.; Chaudhry, G.; Ahmed, S.; *ACS Omega* **2022**, *7*, 3775. [Crossref]
35. Weatherburn, M. W.; *Anal. Chem.* **1967**, *39*, 971. [Crossref]
36. Research Collaboratory for Structural Bioinformatics Protein Data Bank. [Link] accessed in May 2026
37. Laskowski R. A.; MacArthur, M. W.; Moss, D. S.; Thornton, J. M.; *J. Appl. Cryst.* **1993**, *26*, 283. [Crossref]
38. Viana, L. P. S.; Naves, G. M.; Medeiros, I. G.; Guimarães, A. S.; Sousa, E. S.; Santos, J. C. C.; Freire, N. M. L.; de Aquino, T. M.; Modolo, L. V.; de Fátima, Â.; da Silva, C. M.; *Bioorg. Chem.* **224**, *146*, 107247. [Crossref]
39. Costa, N. E. M.; Barreto, T. L.; Freire, N. M. L.; da Silva, J. C. S.; de Aquino, T. M.; Alberto, E. E.; Ishida, K.; de Fátima, Â.; *ACS Omega* **2025**, *10*, 43120. [Crossref]
40. Tavares, M. C.; Nascimento, I. J. S.; de Aquino, T. M.; Brito, T. O.; Macedo Jr., F.; Modolo, L. V.; de Fátima, Â.; Santos, J. C. C.; *Biophys. Chem.* **2023**, *299*, 107042. [Crossref]
41. Warren, G. L.; Andrews, C. W.; Capelli, A.-M.; Clarke, B.; LaLonde, J.; Lambert, M. H.; Lindvall, M.; Nevins, N.; Semus, S. F.; Senger, S.; Tedesco, G.; Wall, I. D.; Woolven, J. M.; Peishoff, C. E.; Head, M. S.; *J. Med. Chem.* **2006**, *49*, 5912. [Crossref]
42. Teague, S. J.; *Nat. Rev. Drug Discovery* **2003**, *2*, 527. [Crossref]
43. De Vivo, M.; Masetti, M.; Bottegoni, G.; Cavalli, A.; *J. Med. Chem.* **2016**, *59*, 4035. [Crossref]
44. Hollingsworth, S. A.; Dror, R. O.; *Neuron* **2018**, *99*, 1129. [Crossref]

Submitted: March 30, 2026
Final version online: May 14, 2026